IEEE Access
Multidisciplinary ⋮ Rapid Review ⋮ Open Access Journal

Received 1 November 2023, accepted 21 November 2023, date of publication 28 November 2023,
date of current version 1 December 2023.

Digital Object Identifier 10.1109/ACCESS.2023.3336694

RESEARCH ARTICLE

Multi-Scenario Stochastic Optimal Scheduling for Power Systems With Source-Load Matching Based on Pseudo-Inverse Laguerre Polynomials

JIAHAO YE, LIRONG XIE, LAN MA, YIFAN BIAN, AND CHUANSHI CUI
School of Electrical Engineering, Xinjiang University, Ürümqi, Xinjiang 830017, China

Corresponding author: Lirong Xie (xielirong@xju.edu.cn)

This work was supported in part by the National Natural Science Foundation of China under Grant 62163034, in part by the Science and Technology Innovation Talents and High-Level Talents Project of the Xinjiang Uygur Autonomous Region under Grant 2022TSYCLJ0017, and in part by the Major Special Project in Xinjiang Uygur Autonomous Region under Grant 2022A01001-1 and Grant 2022A01007-4.

ABSTRACT In the optimization scheduling of power systems containing renewable energy, to ensure that the scheduling results have higher security and better economy, this study proposes a multi-objective forecasting, scenario generation, and decision scheduling integrated stochastic optimal scheduling method. Firstly, to improve the accuracy and stability of wind-photovoltaic power forecasting, a novel multi-objective wind-photovoltaic forecasting model is proposed based on the Laguerre polynomial, pseudo-inverse learning, and hybrid multi-objective Runge-Kutta algorithm (HMORUN). Secondly, to deal with wind-photovoltaic uncertainty, scenarios with representative wind-photovoltaic uncertainty characteristics are generated by scenario generation and reduction techniques using wind-photovoltaic power forecast results. Finally, considering wind-photovoltaic output fluctuations, the degree of source-load matching, wind-photovoltaic utilization, and system economic efficiency factors, with the objective of maximizing the tracking of the load curve and minimizing system economic costs, a stochastic optimized scheduling model for power systems is established. This study uses HMORUN as a solution tool for the multi-objective stochastic optimization scheduling problem (MOSSP). This study uses constraint repair techniques to deal with the complex constraints of the MOSSP model to avoid system load shedding and minimize wind and photovoltaic generation curtailment. To verify the effectiveness of the proposed model, a 10-generator power system, including a wind farm and a photovoltaic plant, is used as a test case for simulation experiments and compared with other multi-objective scheduling models. The experimental results show that the stability of the proposed scheduling model has been improved by a maximum of 0.4%, and the economy has been improved by a maximum of 7.5%.

INDEX TERMS Laguerre polynomial, pseudo-inverse learning, forecasting, hybrid multi-objective Runge-Kutta algorithm, stochastic optimal scheduling.

I. INTRODUCTION

A. MOTIVATION

With the further development of global energy savings, emission reduction, and energy transition, the efficient use of renewable energy has received widespread attention. Among these, the which vigorous development of wind power and photovoltaic power generation is an effective way to realize the energy transition and take the road to sustainable development [1], [2]. Due to the randomness and fluctuation of the output power of wind power and photovoltaic, large-scale wind power and photovoltaic entering the grid will affect the balance of the power system and reduce the reliability of grid operation. Therefore, in the optimal scheduling of power systems containing renewable energy sources, it is important to study how to ensure that the economic costs of power system scheduling are minimized while at the same time maximizing the safety of the scheduling.

The associate editor coordinating the review of this manuscript and approving it for publication was Akin Tascikaraoglu.

B. LITERATURE REVIEW

As an important part of modern smart grid operation and planning, the problem of optimal scheduling of power systems (OSPS) has received widespread attention [3]. The mathematical nature of the OSPS problem is a highly complex nonlinear, multivariate, strongly coupled optimization problem with equation and inequality constraints, and its output curve has a highly non-smooth and non-convex character [4].

Currently, the methods for solving OSPS are generally classified into fuzzy optimal scheduling methods [5], robust optimal scheduling methods [6], and stochastic optimal scheduling methods [7]. Fuzzy optimization scheduling usually converts uncertain optimization problems in power systems into min-max problems, but it has the disadvantage that the membership function is too subjective and the optimization process is not easily interpretable. Robust optimization solves uncertain optimization problems by giving uncertainty sets, which have the disadvantages of overly conservative scheduling results, inflexible decision-making, and high computational complexity [8]. In contrast to the previous two, stochastic optimal scheduling fully considers the uncertainty of renewable energy sources by generating representative scenarios characterizing the uncertainty in the OSPS problem [9]. The more scenarios included in the scenario set, the more uncertain situations are included in the scheduling problem characterized by uncertainty. Therefore, stochastic optimal scheduling is often used as one of the mainstream methods to deal with uncertainty in renewable energy sources [10]. Li et al. [11] proposed a two-stage stochastic optimal scheduling method based on multiple scenarios that achieves flexible handling of uncertainty and economical operation of multi-energy microgrids. Mei et al. [12] proposed a distributed stochastic optimal scheduling model with Latin hypercube sampling and K-means for scene generation and reduction, and the experimental results proved the effectiveness of the proposed method. Staid et al. [13] use non-numerical kernel density estimation to fit historical wind power data to generate probabilistic wind power scenarios and verify the accuracy of the wind power scenarios for stochastic unit combination problems and economic scheduling problems. Lin et al. [14] proposed a stochastic optimal dispatch model based on mean tracking with the objective of minimizing generation costs and tracking errors. The experimental results proved the effectiveness of the proposed model.

In stochastic optimal scheduling, generating high-quality stochastic scenarios can better track wind-photovoltaic uncertainty, but this requires high-quality forecasting in the form of scenarios, and the accuracy of the forecasts directly affects the diversity of the generated scenarios [15], [16]. Chen et al. [17] proposed a scenario generation method based on generative adversarial networks that can capture meteorological features to generate wind-photovoltaic scenarios with fully diverse behaviors. Rayati et al. [18] proposed a Markov chain scenario generation method that takes uncertainty parameters into account for flexible scheduling of active distribution networks. Vagropoulos et al. [19] proposed a method for scenario generation and reduction based on artificial neural networks, which was tested on the Crete power system, and the experimental results showed the effectiveness of the proposed method. Therefore, the use of neural networks for OSPS scenario generation is an effective way to represent the uncertainty of the wind-photovoltaic itself.

Intelligent optimization algorism's parallel search mode has given it powerful non-linear solving capability on multi-objective optimization problems and has been widely used in the field of OSPS [20], [21]. Li et al. [22] proposed a dynamic environmental economic scheduling model that considered tradable green certificates and used a multi-objective moth flame algorithm to solve it. Zhang et al. [2] proposed a multi-objective coordinated scheduling model for hybrid wind-photovoltaic-water generation, and the proposed model was solved by a multi-objective firefly algorithm. Marcelino et al. [23] proposed an optimization model for short-term hydro-generating unit combinations based on a cascade-based operation scenario, which was solved by a multi-objective evolutionary swarm hybridization algorithm. Therefore, it is very effective to use intelligent optimization algorithms to solve multi-objective optimal scheduling problems.

C. RESEARCH GAPS AND QUESTIONS

So far, most wind-photovoltaic forecasting models are single-objective forecasting models, which only consider forecasting accuracy and ignore the impact of improving the stability of forecasting results on the OSPS. Considering both forecasting accuracy and stability can allow the forecasting model to capture more wind-photovoltaic stochastic features so as to ensure more accurate wind-photovoltaic forecasts at the spikes, which can provide more accurate scheduling instructions for OSPS [24]. Therefore, it is necessary to develop new wind-photovoltaic multi-objective forecasting models to provide higher-quality forecasting data for scenario generation, better track the uncertain characteristics of wind-photovoltaic, and ensure the secure and stable operation of the power system.

In addition, the solution objectives of the OSPS model are classified into the following categories: (1) Economic efficiency, including system generation costs and environmental costs, etc., [25] and [26]. (2) System safety, including unit output stability, smoothing of wind-photovoltaic output fluctuations, and tracking of wind-photovoltaic forecast output curves, etc., [27], [28], and [29]. (3) Energy efficiency, including maximum system generation, maximum wind-photovoltaic generation, and minimum system carbon emissions, etc., [30], [31], and [32]. There is a scarcity of research that simultaneously considers wind-photovoltaic output fluctuations, the degree of matching between power output and load, wind-photovoltaic utilization, and system

economic efficiency factors during optimized scheduling. Only by comprehensively considering the coupling relationships among these objectives can the scheduling results be made safer, more economical, and more reliable.

In solving the multi-objective optimization scheduling problem in power systems, traditional optimization methods typically convert the multi-objective problem into a single-objective problem for solution, which cannot well demonstrate the non-dominant relationship between different objectives. Intelligent optimization algorithms possess powerful parallel search capabilities, which make up for the deficiencies of traditional optimization methods. It should be emphasized that although intelligent optimization algorithms have been widely applied in the optimization and scheduling fields, OPDS problems with uncertainty often exhibit complex coupling characteristics, making it difficult for traditional optimization algorithms to find feasible solutions. Therefore, developing novel and effective multi-objective optimization algorithms is highly necessary.

D. NOVELTY AND CONTRIBUTION

The main objective of this research is to develop a multi-objective forecasting, scenario generation, and decision scheduling integrated stochastic optimal scheduling model that ensures maximum security and economy of the scheduling results. The model is divided into three parts: (1) Establishing a new wind-photovoltaic power forecasting model, which is characterized by high forecasting accuracy and strong stability, ensuring a high-quality database for the MOSSP model; (2) A comprehensive consideration of the complex coupling relationship between the source-load targets of the power system to ensure safer, more economical, and more reliable scheduling results; (3) Development of efficient problem-solving tools to effectively solve MOSSP's complex non-linear constraint problems and multi-objective forecasting models. The novelties and contributions of this study are as follows:

(1) The HMORUN algorithm is proposed to solve multi-objective optimization problems. The performance of the HMORUN algorithm is tested on the ZDT test suite and compared with current advanced multi-objective algorithms. Finally, the proposed algorithm is used to optimize a wind-photovoltaic multi-objective forecasting model and a multi-objective stochastic optimized scheduling model.

(2) A hybrid pseudo-inverse Laguerre neural network (HPLNN) is proposed based on pseudo-inverse learning (PIL) and hybrid Laguerre polynomials. The primary aim of HPLNN is to address the overfitting issue that frequently arises in the forecasting process of hybrid Laguerre neural networks (HLNN), which enhances the accuracy and robustness of the forecasting.

(3) A HMORUN-HPLNN multi-objective wind and photovoltaic power forecasting model is proposed based on HMORUN and HPLNN. The main purpose of HMORUN-HPLNN is to improve the accuracy and stability of wind and photovoltaic power forecasting results and provide crucial data foundations for generating representative wind and photovoltaic scenarios.

(4) A HMORUN-MOSSP stochastic optimization scheduling model is established based on HPLLN, HMORUN, Latin hypercube sampling, and simultaneous backward reduction. The HMORUN-MOSSP scheduling model aims to maximize load curve tracking and minimize economic costs while considering the coupling relationship among wind-photovoltaic output fluctuations, the degree of matching between power output and load, wind-photovoltaic utilization, and system economic benefits.

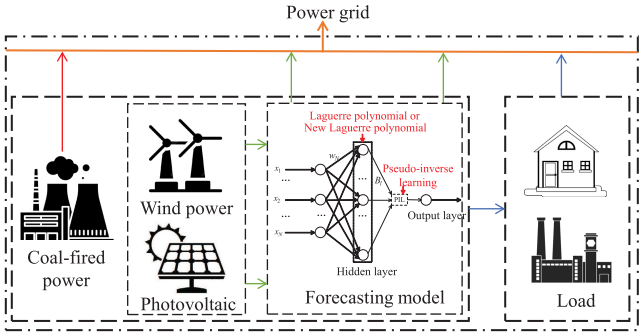

FIGURE 1. MOSSP operating framework.

E. PAPER ORGANIZATION

The rest of this paper is organized as follows: Section II presents the principles of the proposed hybrid pseudo-inverse Laguerre neural network, HMORUN, and the generation of representative scenarios for wind and photovoltaic power. Section III describes the objective function and constraint conditions of the stochastic optimization scheduling model in detail. Section IV elaborates on the selection of experimental data and performance indicators. Section V conducts performance testing experiments on HMORUN, HMORUN-HPLNN, and HMORUN-MOSSP and compares and analyzes the experimental results with those of other models. Section VI summarizes the experimental results of this study. The operational framework of the MOSSP model proposed in this paper is shown in Fig. 1.

II. WIND-PHOTOVOLTAIC MULTI-SCENARIO MODELING

This section describes in detail the methods used in the scene generation process, mainly including the hybrid pseudo-inverse Laguerre neural network, HMORUN, and wind-photovoltaic uncertainty handling methods.

A. WIND-PHOTOVOLTAIC MULTI-OBJECTIVE FORECASTING MODEL CONSTRUCTION

1) HYBRID PSEUDO-INVERSE LAGUERRE NEURAL NETWORK

(1) Hybrid Laguerre neural network Orthogonal polynomials are widely used in constructing feedforward neural networks

due to their strong non-linear approximation capability [33]. Wang et al. [34] proposed a new type of Laguerre polynomial and combined it with the original Laguerre polynomial to form a hybrid Laguerre neural network (HLNN), which exhibited outstanding forecasting performance in wind power forecasting.

The mathematical expressions for the two sets of Laguerre polynomials are described as follows:

$$\begin{cases} P_n(x) = e^x \dfrac{d^n}{dx^n}\left(x^n e^{-x}\right), \ x \in [0, +\infty) \\ NP_n(x) = e^{-x} \dfrac{d^n}{dx^n}\left(x^n e^{x}\right), \ x \in (-\infty, 0] \end{cases} \tag{1}$$

where $P_n(x)$ is a Laguerre orthogonal polynomial whose domain of definition is $[0, +\infty)$. $NP_n(x)$ is a new Laguerre orthogonal polynomial whose domain of definition is $(-\infty, 0]$. The combination of the two Laguerre polynomials extends the domain of definition to $(-\infty, +\infty)$.

The orthogonality of the two sets of Laguerre orthogonal polynomials with respect to the weighting functions is described as follows:

$$\int_0^{\infty} e^{-x} P_n(x) P_m(x)\, dx = \begin{cases} 0, & m \neq n \\ (n!)^2, & m = n \end{cases} \tag{2}$$

$$\int_{-\infty}^{0} e^{x} NP_n(x) NP_m(x)\, dx = \begin{cases} 0, & m \neq n \\ \left(n^2\right)!, & m = n \end{cases} \tag{3}$$

The recurrence equation for two sets of Laguerre orthogonal polynomials is as follows:

$$\begin{cases} P_{n+1}(x) = (1 + 2n - x) P_n(x) - n^2 P_{n-1}(x) \\ NP_{n+1}(x) = (1 + 2n + x) NP_n(x) - n^2 NP_{n-1}(x) \\ (n = 1, 2, \cdots) \end{cases} \tag{4}$$

A mixed neural network constructed with two sets of Laguerre polynomials as orthogonal basis functions improves the applicability of Laguerre neural networks in practical engineering problems [34]. However, feedforward neural networks are prone to overfitting the training data during the training process, which makes it difficult for them to generalize well to new data [35]. Therefore, it is necessary to propose corresponding solutions for this problem.

(2) Pseudo-inverse learning

Pseudo-inverse learning is a technique that can effectively mitigate the overfitting problem in feedforward neural networks [36]. This method leverages the properties of matrix pseudo-inversion to optimize the parameters of the network and improve the accuracy and robustness of its forecasting results. Specifically, pseudo-inverse learning computes the pseudo-inverse matrix of the training data and then multiplies it with the target output vector to obtain the optimal weights. By adopting this approach, the risk of overfitting the neural network is mitigated, leading to improved accuracy and stability in forecasting. The specific process of training HLNN with pseudo-inverse learning is as follows:

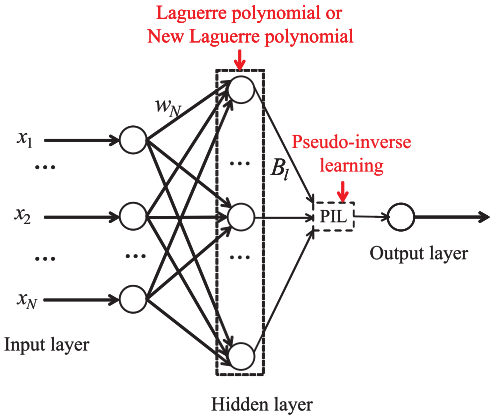

FIGURE 2. Network structure of the hybrid pseudo-inverse Laguerre neural network.

When the input matrix of the training set is $x = [x_1, x_2, \ldots, x_n]$ and the output matrix is $y = [y_1, y_2, \ldots, y_n]$, the HPLNN optimal weight matrix w is calculated as follows:

$$w = \left(X^T X\right)^{-1} X^T y = X^{+} y \tag{5}$$

in which

$$X = \begin{bmatrix} f_1(x_1)\ f_2(x_1)\ \ldots f_m(x_1) \\ f_1(x_2)\ f_2(x_2)\ \ldots f_m(x_2) \\ \ldots \quad \ldots \quad \ldots \quad \ldots \\ f_1(x_n)\ f_2(x_n)\ \ldots f_m(x_n) \end{bmatrix} \tag{6}$$

where X^+ is the Moore-Penrose pseudo-inverse of matrix X, X is the HLNN hidden layer output, and $f(\cdot)$ is the Laguerre orthogonal basis function. The structure of HLNN is shown in Fig. 2.

2) HYBRID MULTI-OBJECTIVE RUNGE-KUTTA ALGORITHM

This study uses HMORUN to optimize the HPLNN wind-photovoltaic forecasting model, which enables the forecasting results to have higher forecasting accuracy and stronger forecasting stability. The proposed HMORUN is a multi-objective version of the Runge-Kutta algorithm [37], and its mechanism for updating non-dominated solutions primarily involves four aspects: updating solutions, enhanced solution quality, and cross-mutation operator. The details of the HMORUN operating mechanism are as follows:

(1) Updating solutions

The update solution strategy of the HMORUN includes two phases: the exploration phase and the exploitation phase, which are executed probabilistically. The detailed update strategy is as follows:

$$\begin{aligned} &if\ rand < 0.5 \\ &\quad (exploration\ phase) \\ &x_{new} = (x_c + r \times SF \times g \times x_c) + SF \times SM + \ldots \\ &\mu \times randn \times (x_m - x_c) \\ &\quad else \\ &\quad (exploitation\ phase) \end{aligned}$$

$$x_{new} = (x_m + r \times SF \times g \times x_m) + SF \times SM + \ldots$$
$$\mu \times randn \times (x_{r1} - x_{r2})$$
$$end \tag{7}$$

where r is an integer that is 1 or -1. SF is an adaptation factor. g and u are random numbers. $randn$ is a random number that follows a normal distribution. x_{r1}, x_{r2}, x_{f1}, and x_{f2} are random solutions of the pareto-frontier (PF). x_m is the current solution for the population.

(2) Enhanced solution quality

The enhanced solution quality strategy consists of three main solution update strategies for x_{new1}, x_{new2}, and x_{new3}, which are described as follows:

$$x_{new1} = \beta \times x_{avg} + (1 - \beta) \times x_{f1} \tag{8}$$

where β is a random number between 0 and 1. x_{avg} is the mean of three random solutions in the PF.

$$\begin{aligned} &if\ rand < 0.5 \\ &\quad if\ w < 1 \\ &x_{new2} = x_{\text{new1}} + r \times w \times |\left(x_{new1} - x_{avg}\right) + randn| \\ &\quad else \\ &x_{new3} = \left(x_{new1} - x_{avg}\right) + r \times w \times |\left(u \times x_{new1} - x_{avg}\right) \\ &\quad + randn| \\ &\quad end \\ &end \end{aligned} \tag{9}$$

where w is a random number. r is an integer of -1, 0, or 1. When $rand < w$, the x_{new3} update strategy is implemented, which is detailed as follows:

$$\begin{aligned} &if\ rand < w \\ &\quad x_{new3} = (x_{new2} - rand \times x_{new2}) + SF \times \\ &\quad \left(rand \times x_{RK} + \left(v \times x_{f1} - x_{new2}\right)\right) \\ &end \end{aligned} \tag{10}$$

where v is a random number that takes the value $2 \times rand$.

(3) Cross-mutation operator

In HMORUN, the cross-mutation operator of NSGAII [38] is introduced. Through performing cross-mutation operations on populations probabilistically to further enhance the exploration and exploitation capabilities of the proposed algorithm. The search mechanism of the cross-mutation operator is as follows:

$$x_{pop} = x_k + \delta \times (u_k - l_k) \tag{11}$$

in which

$$\begin{cases} \phi_1 = (p_k - l_k) / (u_k - l_k) \\ \phi_2 = (u_k - p_k) / (u_k - l_k) \end{cases} \tag{12}$$

If $\theta \leq 0.5$, then δ is:

$$\delta = \left[2\theta + (1 - 2\theta)\left(1 - \phi_1\right)^{\eta_m + 1}\right]^{\frac{1}{\eta_m + 1}} - 1 \tag{13}$$

If $\theta > 0.5$, then δ is:

$$\delta = 1 - \left[2\left(1 - \theta\right) + 2\left(\theta - 0.5\right)\left(1 - \phi_2\right)^{\eta_m + 1}\right]^{\frac{1}{\eta_m + 1}} \tag{14}$$

where x_k is the parent population. θ is a random number between 0 and 1. η is the distribution index.

HMORUN uses the same fast non-dominated sorting and crowding calculation strategy as NSGA-II to select the non-dominated solutions in the population.

Algorithm 1 Local Search Based Algorithm

Input: $Func, N, Maxit, Dim$
Output: P: final population

```
/*initialization*/
Generate initial populations
Calculate Func
/*main loop*/
for it=1:Maxit do
Updating x_new by Eq.(7)
Updating x_new1, x_new2, and x_new3 by Eq.(8), Eq.(9), Eq.(10)
Updating x_pop by Eq.(11)
State ← [x_new1; x_new2; x_new3; x_pop]
P ← bound(State)
P ← Non dominated sorting (N_pop)
P ← Crowding distance calculation (N_pop)
P ← Sort Population selection (N_pop)
it = it + 1
end for
return P
```

This study uses HMORUN to optimize the HPLNN weights and constructs the HMORUN-HPLNN wind-photovoltaic multi-objective forecasting model with accuracy and stability as the optimization objectives. The objective function is shown below:

$$F_a = MSE = \frac{1}{N}\sum_{h=1}^{N}\left(\hat{y}_h - y_h\right)^2 \tag{15}$$

$$F_s = std\left(|\hat{y}_h - y_h|\right), t = 1, 2, \ldots, N \tag{16}$$

where F_a is the forecast accuracy index. F_s is the forecast stability index. $\hat{y}_h$, y_h, and N are the forecast values, actual values, and sample numbers for wind and photovoltaic, respectively.

B. WIND-PHOTOVOLTAIC UNCERTAINTY HANDLING

In this paper, the uncertainty in the behavior of renewable energy sources is fully taken into account, and the uncertainty in wind power and photovoltaic is treated in three ways.

Firstly, a stochastic optimization approach is used to deal with the uncertainty of renewable energy. In the stochastic optimization approach, the uncertainty of renewable energy is characterized by generating representative wind and photovoltaic power generation scenarios. The more scenarios are included in the set of scenarios, the more

uncertain situations are included in the scheduling problem characterized by uncertainty. In this paper, Latin hypercube sampling (LHS) [39] and imultaneous backward reduction (SBR) [40] are used to generate representative wind-photovoltaic scenarios. Secondly, generating high-quality stochastic scenarios can better track the wind-photovoltaic uncertainty, but this is based on accurate and high-quality forecasting, and the accuracy of forecasting directly affects the diversity of generated scenarios. Therefore, this paper proposes a new multi-objective forecasting model for wind and photovoltaic so that the forecasting model captures more stochastic features of wind-photovoltaic, which ensures more accurate wind-photovoltaic forecasts at "peak" moments and provides a high-quality data base for generating characteristic scenarios. Finally, the effects of wind and photovoltaic fluctuations are taken into account in the system rotation standby capacity to improve the reliability of the power system.

III. PROBLEM DESCRIPTION OF STOCHASTIC OPTIMAL SCHEDULING

This study proposes a multi-objective stochastic optimal scheduling model that fully considers the impact of wind-photovoltaic uncertainty on power system scheduling. This section mainly describes the problem of the proposed model, including relevant objective functions and constraints, which are shown below.

A. OBJECTIVE FUNCTION

(1) Source-load difference index

One of the focuses of coordinated source-load scheduling is to minimize the difference between the power-side output curve and the load curve to ensure the safe and stable operation of the power system. Therefore, this study employs the source-load difference index (SLDI) as one of the objectives of the proposed scheduling model, which is expressed mathematically as follows:

$$\begin{cases} \min F_{si} = \alpha_1 Q_P + \alpha_2 Q_L + \alpha_3 Q_\theta \\ \alpha_1 + \alpha_2 + \alpha_3 = 1 \end{cases} \tag{17}$$

where F_{si} is the source-load difference index. Q_P, Q_L, and Q_θ are the standard deviation of the power-side output fluctuations, the standard deviation of the residual load, and the standard deviation of the curve corner, respectively. α_1, α_2, and α_3 are the weighting factors.

$$\begin{cases} P_{s,t} = P_t + P_{w,t} + P_{v,t} \\ Q_P = \sqrt{\dfrac{1}{T}\sum_{t=1}^{T}\left(P_{s,t} - \bar{P}_s\right)^2} \end{cases} \tag{18}$$

where P_t, $P_{w,t}$, and $P_{v,t}$ are the output power of units, wind farms, and photovoltaic plants, respectively, at time t. $P_{s,t}$ is the total power on the power side at time t. T is the total scheduling time.

$$\begin{cases} C_{L,t} = P_{loss,t} + P_{L,t} - P_{s,t} \\ Q_L = \sqrt{\dfrac{1}{T}\sum_{i=1}^{T}\left(C_{L,t} - \bar{C}_L\right)^2} \end{cases} \tag{19}$$

where $P_{L,t}$ and $C_{L,t}$ are the load and residual load at time t, respectively. $P_{loss,t}$ is the system network loss at time t.

$$Q_\theta = \sqrt{\frac{1}{T}\sum_{t=1}^{T}\left(\theta_t - \bar{\theta}_t\right)^2} \tag{20}$$

$$k_t = \begin{cases} \dfrac{P_{s,t+1} - P_{s,t}}{t\,(t+1) - t\,(t)} & (1 \le t \le T-1) \\ \dfrac{P_{s,T} - P_{s,T-1}}{t\,(T) - t\,(T-1)} & (t = T) \end{cases} \tag{21}$$

If $t = 1, t = T$, then θ_t is:

$$\theta_t = \arctan|k_t| \tag{22}$$

If $k_t k_{t-1} \ge 0, 2 \le t \le T-1$, then θ_t is:

$$\theta_t = |\arctan k_t - \arctan k_{t-1}| \tag{23}$$

If $k_t k_{t-1} < 0, 2 \le t \le T-1$, then θ_t is:

$$\theta_t = \arctan|k_t| + \arctan|k_{t-1}| \tag{24}$$

where θ_t and k_t are the corner of two adjacent polyline segments and the slope of the polyline segment at time t, respectively.

(2) Economic costs

Taking into account the impact of various factors on the economic costs of the proposed model, minimizing the total economic cost of the system is another optimization objective of MOSSP. In order to accurately reflect the actual operating costs of thermal power units, this study considers the fuel cost and valve-point effect (VPE) cost of the power generation units. To maximize the utilization of wind and photovoltaic power and reduce the curtailment of wind and photovoltaic power as well as the system load shedding, this study also takes into account the overestimation cost and underestimation cost of wind and photovoltaic power. The mathematical expression for the comprehensive economic cost F_{ec} is as follows:

$$\begin{aligned} \min F_{ec} = &\sum_{t=1}^{T}\sum_{n=1}^{N} F\left(P_{n,t}\right) + \sum_{t=1}^{T}\sum_{n=1}^{N} E\left(P_{n,t}\right) \\ &+ \sum_{t=1}^{T}\left(c_{wv}E_{c,t} + l_{wv}E_{l,t}\right) \end{aligned} \tag{25}$$

where $F\left(P_{n,t}\right)$ and $E\left(P_{n,t}\right)$ are unit fuel costs and VPE costs at time t. c_{wv} and l_{wv} are underestimated cost factors and overestimated cost factors. $E_{c,t}$ and $E_{l,t}$ are wind-photovoltaic electricity abandonment and load shedding at time t. The equations for $F\left(P_{n,t}\right)$ and $E\left(P_{n,t}\right)$ are as follows:

$$F\left(P_{n,t}\right) = a_n P_{n,t}^2 + b_n F P_{n,t} + c_n \tag{26}$$

$$E\left(P_{n,t}\right) = \left|d_n \sin\left[e_n\left(P_{n,\min} - P_{n,t}\right)\right]\right| \tag{27}$$

In the n-th thermal generator, a_n, b_n, and c_n are fuel cost coefficients. d_n and e_n are VPE cost coefficients. $P_{n,t}$ is the output power at time t. $P_{n,min}$ is the lower limit of the generator set output power.

B. CONSTRAINTS

(1) Power balance constraints

The power balance constraint of MOSSP is expressed as an equation constraint, and its mathematical expression is as follows:

$$\sum_{n=1}^{N} P_{n,t} + P_{w,t} + P_{v,t} = P_{loss,t} + P_{load,t} \tag{28}$$

in which

$$P_{loss,t} = \sum_{i=1}^{N}\sum_{j=1}^{N} P_{i,t}B_{i,j}P_{j,t} + \sum_{i=1}^{N} P_{i,t}B_{i,0} + B_{0,0} \tag{29}$$

where $B_{i,j}$, $B_{i,0}$, and $B_{0,0}$ are the network loss coefficients.

(2) Generator capacity constraints

$$P_{n,\min} < P_{n,t} < P_{n,\max} \tag{30}$$

where $P_{n,max}$ and $P_{n,min}$ are the maximum and minimum output power of the nth generator.

(3) Generating unit ramp-rate constraints

$$\begin{cases} P_{n,t} - P_{n,t-1} < UR_n \\ P_{n,t-1} - P_{n,t} < DR_n \end{cases} \tag{31}$$

where UR_n and DR_n are the maximum power rising and falling per unit time of the n-th generator in the MOSSP, respectively.

(4) Rotating standby capacity constraint

The integrated consideration of wind power, PV, and load fluctuations is helpful to ensure the safe and stable operation of the MOSSP. The positive and negative rotation standby constraints for the system are as follows:

$$\begin{cases} P_{w,t} \times w_u\% + P_{v,t} \times w_u\% + P_{load,t} \times L_u\% \le \sum_{n=1}^{N} U_{n,t} \\ \left(P_{w,\max} + P_{v,\max} - P_{w,t} - P_{v,t}\right) \times w_d\% \le \sum_{n=1}^{N} D_{n,t} \end{cases} \tag{32}$$

in which

$$\begin{cases} U_{n,t} = \min\left(P_{n,\max} - P_{n,t}, UR_n\Delta T\right) \\ D_{n,t} = \min\left(P_{n,t} - P_{n,\min}, DR_n\Delta T\right) \end{cases} \tag{33}$$

where $w_u\%$, $w_d\%$, and $L_u\%$ are the fluctuation coefficients of wind-photovoltaic power and load in the positive and negative rotating standby capacities, respectively. $P_{w,max}$ and $P_{v,max}$ are the rated power of the wind farm and photovoltaic plant. ΔT is the rotating standby response time, which takes $\Delta T = 1/6$ hour in this paper.

When the actual wind-photovoltaic output is greater than the demand of the scheduling plan and the negative rotating standby capacity of the system cannot offset this power, wind, and photovoltaic abandonment will only occur. The system underestimation is calculated as follows:

$$E_{c,t} = \left|P_{loss,t} + P_{L,t} - \left(P_t + P_{w,t} + P_{v,t}\right)\right| - \sum_{n=1}^{N} D_{n,t} \tag{34}$$

When the actual wind-photovoltaic output is less than the demand of the scheduling plan and the system's reserved positive rotating standby capacity cannot supplement this power deficit, load shedding will only occur. The system overestimate is calculated as follows:

$$E_{l,t} = P_{loss,t} + P_{L,t} - \left(P_t + P_{w,t} + P_{v,t}\right) - \sum_{n=1}^{N} U_{n,t} \tag{35}$$

This study utilizes HMORUN to solve the MOSSP and constructs the HMORUN-MOSSP stochastic optimized scheduling model, which mainly includes wind-photovoltaic multi-objective forecasting, scenario generation and reduction, as well as stochastic scheduling model solving. The flow chart of the proposed stochastic optimal scheduling model is shown in Fig. 3.

IV. DATA COLLECTION AND PERFORMANCE CRITERIA

This section describes in detail the wind power data, photovoltaic data, load data, and indicators for the evaluation of the experimental results that were used in the course of the experiments.

A. DATA COLLECTION

In this study, wind and photovoltaic data were obtained from a wind farm and a photovoltaic plant in Hami, Xinjiang. The load data were obtained from the 10-generator power system [41]. This study collected historical data from wind farms and photovoltaic plants for January (the sampling point time interval is 1 h). Wind farm data includes wind speed, wind direction, temperature, barometric pressure, humidity, and power. The photovoltaic plant data include irradiation intensity, temperature, barometric pressure, relative humidity, and power. The first 29 days of January (696 samples) were used for training, and the 30th day's samples (24 samples) were used for testing to verify the performance of the proposed HMORUN-HPLNN wind and photovoltaic forecasting models. Historical power data for wind farms and photovoltaic plants are shown in Fig. 4.

B. PERFORMANCE CRITERIA

This study uses stability index (SDEX), mean absolute error (MAE), root mean square error (RMSE), index of agreement (IA), and median absolute percentage error (MdAPE) as evaluation indicators of the forecasting model to comprehensively evaluate the forecasting accuracy and forecasting stability of the HMORUN-HPLNN forecasting

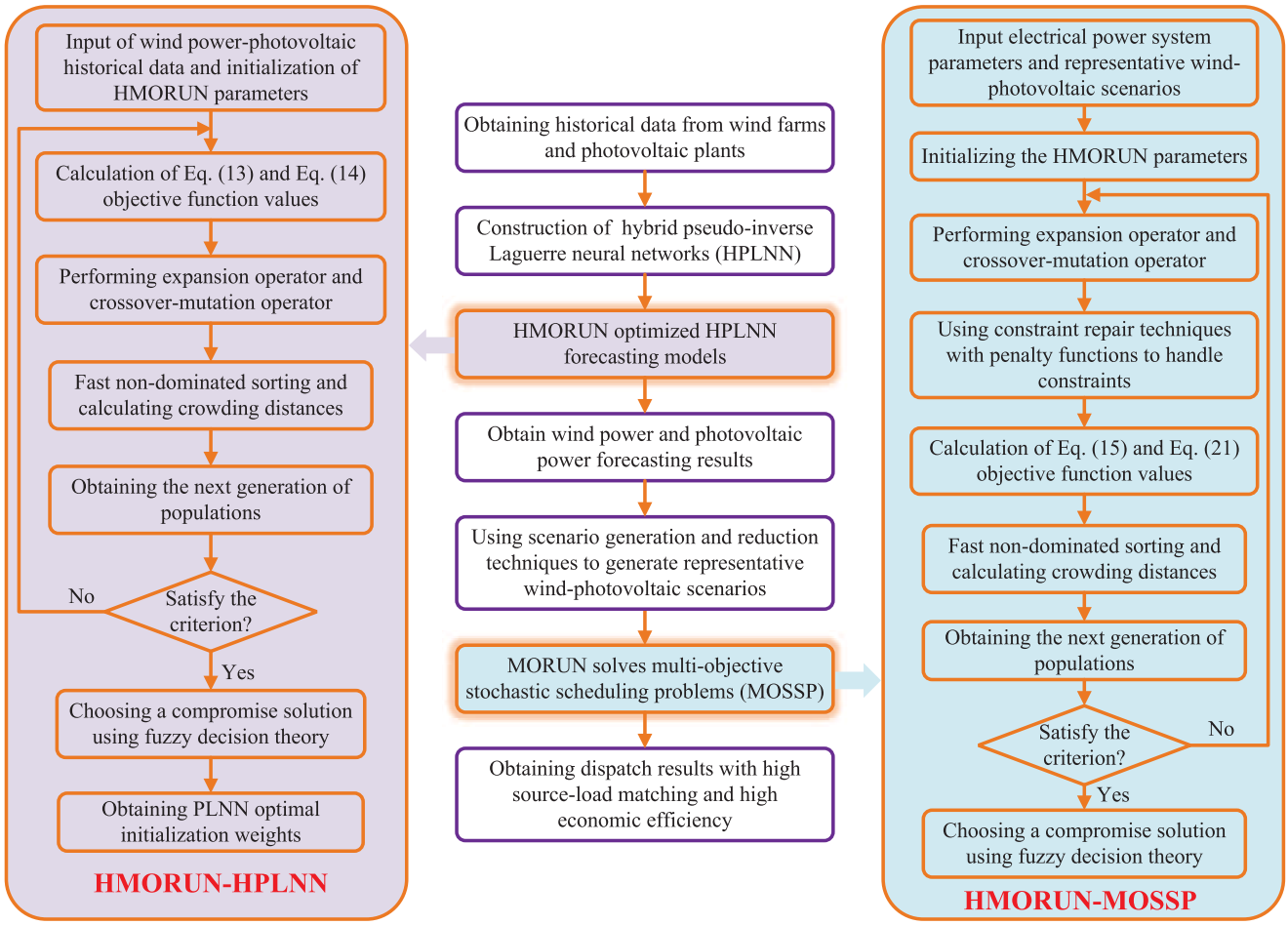

FIGURE 3. Flow chart of the proposed stochastic optimal scheduling model.

model [24]. SDEX reflects the degree of stability of the model forecast. MAE reflects the overall level of error. RMSE reflects the degree of difference between the forecasted and actual values. IA reflects the sensitivity and proportional change of the difference between the forecasted and actual values. MdAPE responds to the forecasting accuracy of the model. The mathematical formula for the evaluation indicators is as follows:

$$SDEX = std\left(\left|\hat{y}_h - y_h\right|\right) \tag{36}$$

$$MAE = \frac{1}{N}\sum_{h=1}^{N}\left|\hat{y}_h - y_h\right| \tag{37}$$

$$RMSE = \sqrt{\frac{1}{N}\sum_{h=1}^{N}\left(\hat{y}_h - y_h\right)^2} \tag{38}$$

$$IA = 1 - \frac{\sum_{h=1}^{N}\left(\hat{y}_h - y_h\right)^2}{\sum_{h=1}^{N}\left(\left|\hat{y}_h - \bar{y}_h\right| + \left|y_h - \bar{y}_h\right|\right)^2} \tag{39}$$

$$MdAPE = median\left(\left|\frac{\hat{y}_h - y_h}{y_h}\right| \times 100\%\right) \tag{40}$$

where $\bar{y}_h$ is the mean of the actual values of the test sample.

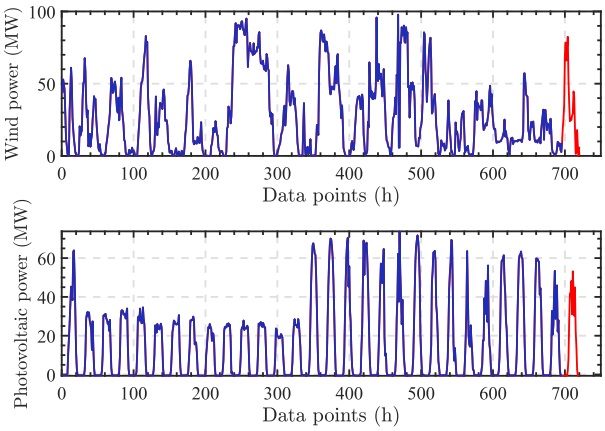

FIGURE 4. Wind and photovoltaic power data for HMORUN-HPLNN.

V. EXPERIMENTAL RESULTS AND ANALYSIS

To verify the effectiveness of the proposed multi-objective forecasting, scenario generation, and decision scheduling integrated stochastic optimal scheduling model, this section conducts extensive integrated experiments on the HMORUN algorithm, the HMORUN-HPLNN wind and photovoltaic power forecasting model, and the HMORUN-MOSSP

TABLE 1. Definition of test functions ZDT1-ZDT4.

ZDT1: Minmize: $f_1 = x_1$ Minmize: $f_2 = g(x)\left[\sqrt{1 - x_1/g(x)}\right]$ $g(x) = 1 + 9\left(\sum_{i=2}^{n} x_i\right)/(n-1)$	ZDT2: Minmize: $f_1 = x_1$ Minmize: $f_2 = g(x)\left[1 - (x_1/g(x))^2\right]$ $g(x) = 1 + 9(\sum_{i=2}^{n} x_i)/(n-1)$
ZDT3: Minmize: $f_1 = x_1$ Minmize: $f_2 = g(x)\left[\sqrt{1 - x_1/g(x)} - \frac{x_1}{g(x)}\sin(10\pi x_1)\right]$ $g(x) = 1 + 9(\sum_{i=2}^{n} x_i)/(n-1)$	ZDT4: Minmize: $f_1 = x_1$ Minmize: $f_2 = g(x)\left[\sqrt{1 - x_1/g(x)}\right]$ $g(x) = 1 + 10(n-1) + \sum_{i=2}^{n}\left[x_i^2 - 10\cos(4\pi x_i)\right]$

TABLE 2. IGD values obtained by MOALO, MODA, NSGAIII, MOSSA, MORUN, and HMORUN on ZDT1-ZDT4 with Dim=10.

Algorithms	ZDT1					Algorithms	ZDT2				
	Best	Mean	Median	Std	Worst		Best	Mean	Median	Std	Worst
MOALO	0.0644	0.1293	0.1290	0.0417	0.1707	MOALO	0.1037	0.3396	0.2502	0.2046	0.6010
MODA	0.3860	0.5825	0.6082	0.1426	0.7275	MODA	0.0163	0.0835	0.0300	0.1166	0.2579
NSGAIII	0.0179	0.0356	0.0416	0.0112	0.0439	NSGAIII	0.0273	0.0399	0.0402	0.0092	0.0532
MOSSA	0.0180	0.0297	0.0270	0.0110	0.0477	MOSSA	0.0173	0.0201	0.0192	0.0027	0.0243
MORUN	0.0060	0.0068	0.0062	0.0011	0.0087	MORUN	0.0056	0.0073	0.0077	0.0015	0.0092
HMORUN	**0.0045**	**0.0047**	**0.0047**	**0.0002**	**0.0049**	HMORUN	**0.0046**	**0.0048**	**0.0047**	**0.0003**	**0.0051**
Algorithms	ZDT3					Algorithms	ZDT4				
	Best	Mean	Median	Std	Worst		Best	Mean	Median	Std	Worst
MOALO	0.0282	0.0465	0.0370	0.0233	0.0854	MOALO	0.3967	0.4145	0.4211	0.0149	0.4294
MODA	0.3431	0.4787	0.4746	0.1438	0.6226	MODA	1.6105	1.6191	1.6234	0.0079	1.6255
NSGAIII	0.4546	0.5734	0.5127	0.1287	0.7418	NSGAIII	0.5416	0.7065	0.7585	0.1135	0.7983
MOSSA	0.0332	0.0442	0.0464	0.0094	0.0530	MOSSA	0.0290	0.3179	0.1912	0.3920	0.9752
MORUN	0.0155	0.0241	0.0261	0.0069	0.0331	MORUN	0.0046	0.0060	0.0049	0.0019	0.0091
HMORUN	**0.0049**	**0.0051**	**0.0051**	**0.0002**	**0.0054**	HMORUN	**0.0044**	**0.0045**	**0.0045**	**0.0002**	**0.0047**

Note: The values in bold indicate the best IGD values.

scheduling model. Firstly, the performance of the HMORUN algorithm is tested on the ZDT test suite [24] and compared with other advanced multi-objective algorithms. Secondly, the HMORUN-HPLNN wind power and photovoltaic power forecasting models were tested, including HMORUN-HPLNN forecasting performance testing and comparison of multi-model forecasting results. Finally, the HMORUN-MOSSP scheduling model was tested, including parameter sensitivity analysis, HMORUN-MOSSP scheduling capability testing, and comparison of multi-model optimization scheduling results. Each experiment was independently run 30 times, and the average of the 30 experiment results was compared, and the best value of PF was selected from the 30 experiment results for comparison.

A. TESTING OF HMORUN

To verify the performance of the proposed HMORUN algorithm, it was compared with advanced multi-objective algorithms such as MOALO [42], MODA [43], NSGAIII [44], MOSSA [45], and MORUN [24] on the ZDT test suite. The ZDT test suite consists of four benchmark problems (ZDT1-ZDT4) with 10 dimensions, and their objective functions are presented in Table 1. The parameter settings for the five comparison algorithms were taken from the original literature. For HMORUN, the population size is set to 100, and the maximum number of function evaluations is set to 1E+04, which is consistent with the other algorithms. The inverted generational distance (IGD) is used to evaluate the convergence and distribution performance of the algorithms. The statistical results of IGD for all six algorithms are shown in Table 2, and the best non-dominated solutions are presented in Fig. 5.

Table 2 compares the experimental results of six algorithms using evaluation indicators such as best value, average value, median, standard deviation (std), and worst value. The results show that the proposed HMORUN algorithm obtains the best IGD value on ZDT1-ZDT4 test problems. From Fig. 5, it can be seen that the non-dominated solutions of HMORUN are closer to the true Pareto front on ZDT1-ZDT4 compared to MOALO, MODA, NSGAIII, MOSSA, and MORUN algorithms. Additionally, the non-dominated solutions obtained by HMORUN are more uniformly distributed and have a higher distribution density than the compared algorithms. Hence, the proposed HMORUN algorithm outperforms MOALO, MODA, NSGAIII, MOSSA, and MORUN in terms of performance.

B. TESTING HMORUN-HPLNN WIND-PHOTOVOLTAIC FORECASTING MODELS

1) TESTING OF HMORUN-HPLNN

To verify the performance of the proposed HPLNN forecasting model, two forecasting models are designed in this section

for comparison experiments. The two forecasting models are HMORUN-HLNN and HMORUN-HPLNN, respectively. HMORUN population N=100, PF size NPF=100, number of function evaluations FEs=1E+4.

To ensure the fairness of comparative experiments, firstly, HMORUN is used to optimize the initial weights of both HLNN and HPLNN, ensuring that the two forecasting models have the same initial weights. Then, the optimized initial weights are assigned to HLNN and HPLNN for wind and photovoltaic power forecasting. The results of the wind and photovoltaic power forecasts and the PF obtained by HMORUN are shown in Fig. 6, and the statistical results of the evaluation indicators are shown in Table 3.

The results shown in Fig. 6 and Table 3 demonstrate that the HMORUN-HPLNN forecasting model outperforms the HMORUN-HLNN forecasting model in wind and photovoltaic power forecasting, as evidenced by its superior evaluation metrics. These findings suggest that the proposed HPLNN is able to address the limitations of traditional feed-forward neural networks, thereby improving the forecasting performance of the model.

2) FORECASTING RESULTS OF MODELS WITH DIFFERENT MULTI-OBJECTIVE ALGORITHMS

To verify the effectiveness of the proposed HMORUN in optimizing wind and photovoltaic forecasting models, HMORUN is compared with state-of-the-art multi-objective optimization algorithms, including NSGAIII, MOSSA, MODA, MOALO, and MORUN, for the wind-photovoltaic power forecasting problem. The experimental comparison results are shown in Fig. 7, Table 4, and Table 5.

Based on Fig. 7 (a) and Table 4, it is evident that the HMORUN-HPLNN wind power forecasting model proposed in this study outperforms other models in the field of wind power forecasting. Compared with the MOALO-HPLNN, MODA-HPLNN, NSGAIII-HPLNN, MOSSA-HPLNN, and MORUN-HPLNN wind power forecasting models, HMORUN-HPLNN achieved better evaluation index values and higher forecasting fit. As a result, the proposed wind power forecasting model exhibits superior forecasting performance. HMORUN provides a more effective solution to the wind power forecasting problem.

Based on Fig. 7 (b) and Table 5, it is evident that the HMORUN-HPLNN photovoltaic power forecasting model proposed in this study exhibits superior forecasting performance and evaluation index values in the field of photovoltaic power forecasting. Specifically, although the MOSSA-HPLNN photovoltaic power forecasting model achieved the best evaluation index values in terms of MAE, the HMORUN-HPLNN forecasting model outperformed the other five models in terms of IA, RMSE, and SDEX, and exhibited a better fit. As such, the proposed HMORUN-HPLNN photovoltaic power forecasting model exhibits superior forecasting performance. HMORUN provides a more effective solution to the photovoltaic power forecasting problem.

3) FORECASTING RESULTS OF DIFFERENT NEURAL NETWORK MODELS

To further evaluate the forecasting performance of the proposed HMORUN-HPLNN wind-photovoltaic forecasting model, which is compared with the current popular neural network forecasting models (including machine learning and deep learning models). The main forecasting models used for comparison include BPNN [46], LSTM [47], WNN [48], RELM [49], and HLNN. For a fair comparison, combine them with HMORUN to construct HMORUN-BPNN, HMORUN-LSTM, HMORUN-WNN, HMORUN-RELM, and HMORUN-HLNN forecasting models. The parameters of HMORUN are set as described in the section ''1) Testing of HMORUN-HPLNN''. Neural network parameters are determined through cross-validation. The maximum function evaluation times for each forecasting model are set as FEs=1E+04. The experimental comparison of the forecasting models is run independently 30 times, and their average values are taken as the final experimental results. The results of the experimental comparison of wind and PV power forecasts are shown in Table 6 and Table 7.

The comparative analysis of the results between Table 6 and Table 7 demonstrates that, in contrast to forecasting models such as HMORUN-BPNN, HMORUN-LSTM, HMORUN-WNN, HMORUN-RELM, and HMORUN-HLNN, the evaluation metrics for HMORUN-HPLNN exhibit a distinct advantage. This indicates that the proposed forecasting model boasts higher accuracy and superior stability.

C. GENERATION OF WIND-PHOTOVOLTAIC REPRESENTATIVE SCENARIOS

First, 1000 wind and photovoltaic scenarios were generated using LHS based on the wind and photovoltaic power forecasts, respectively. Then, SBR was applied to reduce the number of scenarios and probabilistically generate five representative scenarios for wind and photovoltaic. The sample sampling rate for wind and PV power is 1 h. The probabilities of generating the five representative scenarios for wind and photovoltaic were 0.103, 0.181, 0.113, 0.374, and 0.229, respectively. Fig. 8 shows the generation and reduction results for the wind and photovoltaic scenarios.

D. TESTING OF THE HMORUN-MOSSP

To validate the performance of the proposed randomized optimization scheduling model, we conducted comprehensive experiments on the HMORUN-MOSSP model. The experiments primarily included sensitivity analysis of weight coefficients, performance testing of HMORUN-MOSSP scheduling, and comparison of multi-model optimal scheduling results.

1) WEIGHTING FACTORS SENSITIVITY ANALYSIS

This subsection focuses on the optimal ratio of weighting factors α_1, α_2, and α_3 in SLDI. The weighting factors α_1,

TABLE 3. Statistics of wind-photovoltaic power forecasting results of two neural networks.

Wind power	Evaluation metrics				
	IA	MAE	RMSE	SDEX	MdAPE
MORUN-HLNN	0.9963	2.5663	2.8727	**1.2795**	8.9575
MORUN-HPLNN	**0.9968**	**2.0579**	**2.6722**	1.7368	**5.9587**
Photovoltaic	Evaluation metrics				
	IA	MAE	RMSE	SDEX	MdAPE
MORUN-HLNN	0.9744	4.1066	6.3381	4.9310	59.8132
MORUN-HPLNN	**0.9963**	**1.7805**	**2.3713**	**1.5996**	**40.0019**

Note: The values in bold indicate the best evaluation metrics values.

TABLE 4. Statistics of wind power forecasting results for six forecasting models.

Models	Evaluation metrics				
	IA	MAE	RMSE	SDEX	MdAPE
MOALO-HPLNN	0.9431	7.6394	9.5366	5.8313	20.0955
MODA-HPLNN	0.9232	9.1626	10.7824	5.8062	25.0564
NSGAIII-HPLNN	0.9702	8.0043	8.5122	2.9584	25.7654
MOSSA-HPLNN	0.8882	3.0997	6.7786	5.0712	43.4111
MORUN-HPLNN	0.9841	3.3904	4.3231	2.6422	9.4020
HMORUN-HPLNN	**0.9968**	**2.0579**	**2.6722**	**1.7368**	**5.9587**

Note: The values in bold indicate the best evaluation metrics values.

TABLE 5. Statistics of photovoltaic power forecasting results for six forecasting models.

Models	Evaluation metrics				
	IA	MAE	RMSE	SDEX	MdAPE
MOALO-HPLNN	0.9927	2.7875	3.3453	1.8893	42.1236
MODA-HPLNN	0.9912	2.967	3.787	2.4039	41.3944
NSGAIII-HPLNN	0.9738	4.3176	6.4501	4.895	54.1213
MOSSA-HPLNN	0.9673	**1.1989**	3.5225	5.2829	52.4322
MORUN-HPLNN	0.9763	3.8902	6.0855	4.7802	61.6205
HMORUN-HPLNN	**0.9963**	1.7805	**2.3713**	**1.5996**	**40.0019**

Note: The values in bold indicate the best evaluation metrics values.

α_2, and α_3 are the main parameters affecting the value of SLDI. Under the constraint of $\alpha_1 + \alpha_2 + \alpha_3 = 1$, a total of 19 comparative experiments from $\alpha_1 : \alpha_2 : \alpha_3 = 1 : 1 : 1$ to $\alpha_1 : \alpha_2 : \alpha_3 = 8 : 1 : 8$ are set up to discuss the optimal values of α_1, α_2, and α_3. The comparative results of the experiments with different weighting ratios of α_1, α_2, and α_3 are shown in Table 8.

As can be seen in Table 8, the SLDI values vary with the weighting factors α_1, α_2, and α_3. Overall, the SLDI values decrease when the single weighting factor increases. The decreasing effect of SLDI values becomes greater when the double-weighting factors are increased simultaneously. However, as the weighting factors increase beyond a certain threshold, the SLDI values start to deteriorate. The SLDI values are minimized when the α_1, α_2, and α_3 weight ratios are 1, 8, and 8, respectively. Therefore, the values of α_1, α_2, and α_3 in this study are 0.059, 0.470, and 0.471, respectively.

2) PERFORMANCE TESTING OF HMORUN-MOSSP

This subsection focuses on testing the performance of the HMORUN-MOSSP stochastic optimization scheduling model. Five representative wind and photovoltaic scenarios are used as input to the MOSSP model, and the MOSSP model is solved using HMORUN with the SLDI and economic cost as the objective functions. The HMORUN-MOSSP scheduling model ensures both safety and economy of scheduling results while also minimizing the amount of wind and photovoltaic power curtailment and load shedding. The PF and the optimal compromise output power of the units of the HMORUN-MOSSP model are shown in

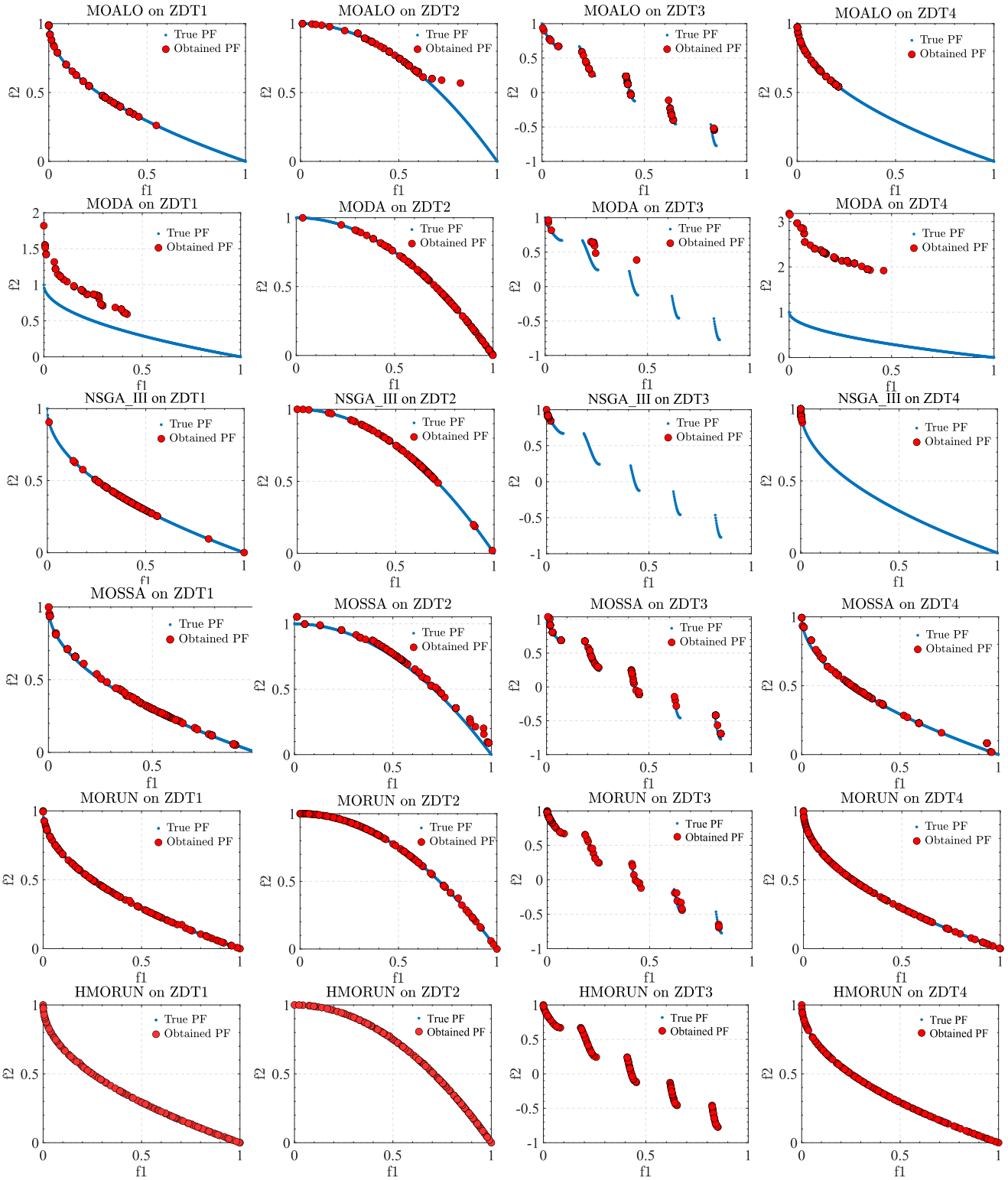

FIGURE 5. Obtained Pareto optimal solutions by MOALO, MODA, NSGAIII, MOSSA, MORUN, and HMORUN on ZDT1-ZDT4.

Fig. 9, and the optimal compromise solution output results for 24 hours are shown in Table 9.

Based on Fig. 9 (a), it can be observed that the non-dominated solutions obtained by the HMORUN-MOSSP scheduling model are uniformly distributed with high density, indicating that HMORUN has good global exploration capability for MOSSP. The shape of the PF distribution tends towards a straight line, which indicates that HMORUN has a

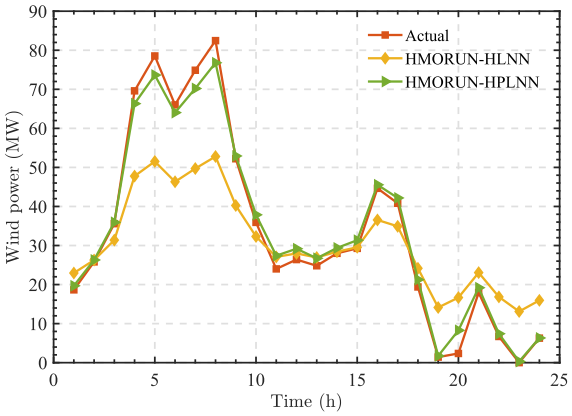

(a) Wind power forecast comparison curves

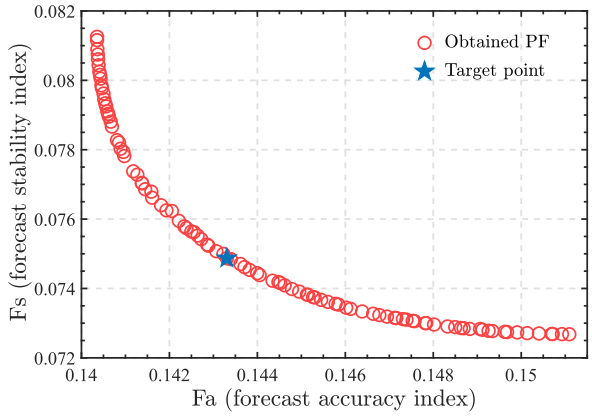

(b) Compromise solutions obtained by HMORUN in wind power forecasting

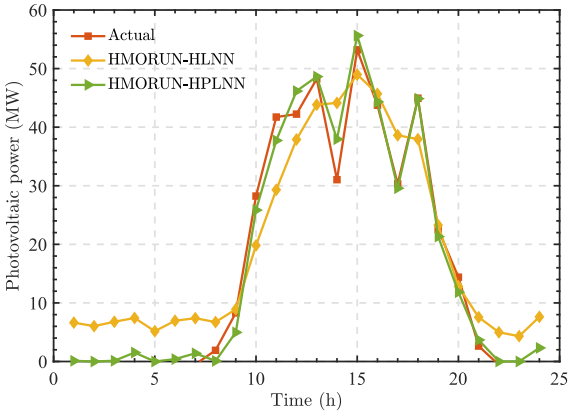

(c) Photovoltaic power forecast comparison curves

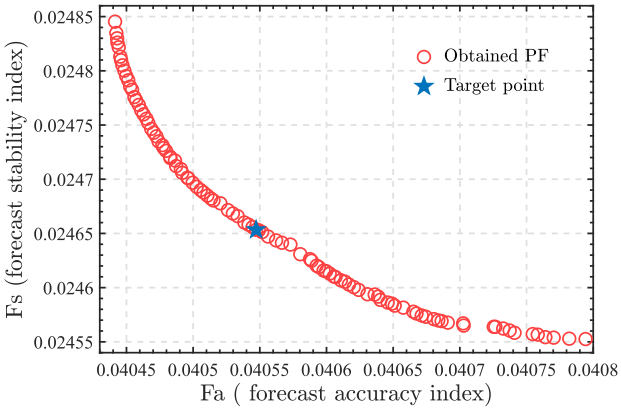

(d) Compromise solution obtained by HMORUN in photovoltaic power forecasting

FIGURE 6. **Comparison of PF and forecasting curves for wind and photovoltaic power forecasting from two neural networks.**

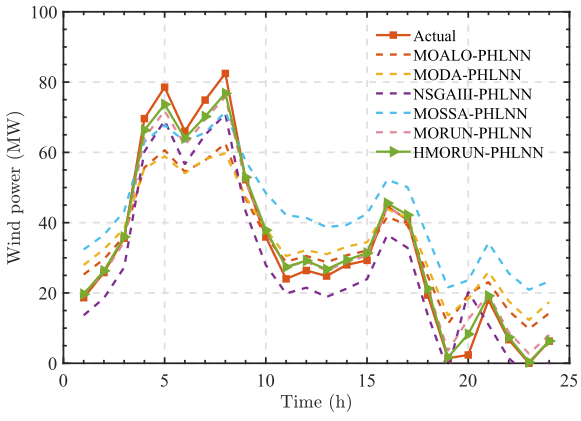

(a) Wind power forecast comparison curves

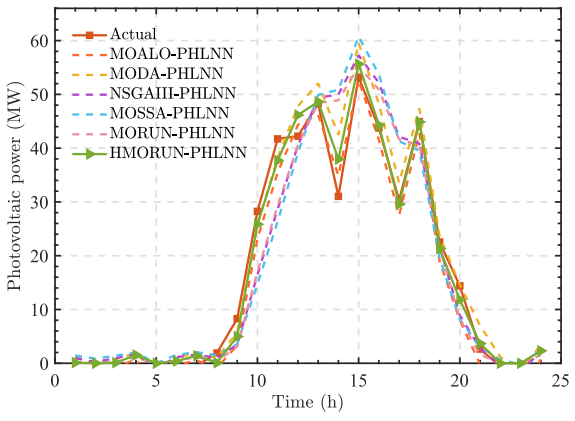

(b) Photovoltaic power forecast comparison curves

FIGURE 7. **Comparison curves of six wind and photovoltaic power forecasting models.**

good solving capability for MOSSP and is able to find a better non-dominated solution for it.

Based on Fig. 9 (b) and Table 9, it can be seen that the balancing constraints of the HMORUN-MOSSP model have been satisfied. This indicates that the proposed model can ensure both safety and economic considerations in the scheduling results while avoiding curtailment of wind and solar power and load shedding. Therefore,

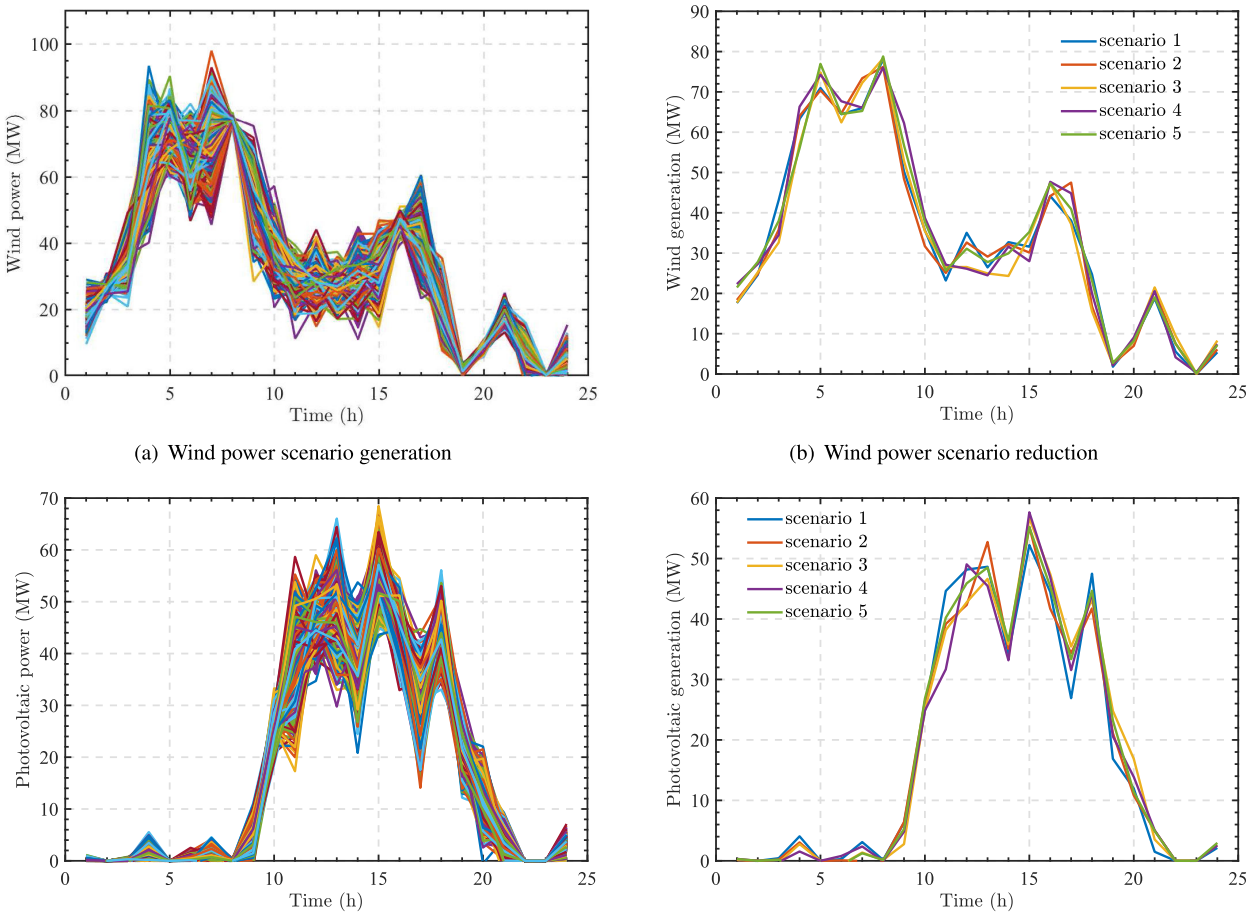

(a) Wind power scenario generation

(b) Wind power scenario reduction

(c) Photovoltaic power scenario generation

(d) Photovoltaic power scenario reduction

FIGURE 8. Wind and photovoltaic power scenario generation and reduction.

TABLE 6. Statistics on wind power forecasting results of six neural network forecasting models.

Models	Evaluation metrics				
	IA	MAE	RMSE	SDEX	MdAPE
HMORUN-BPNN	0.9839	4.7534	5.7096	3.1009	12.1455
HMORUN-LSTM	0.9958	2.7167	3.0893	1.5019	7.9351
HMORUN-WNN	0.9857	4.1195	5.5825	3.8486	8.6357
HMORUN-RLEM	0.9831	4.8589	5.8466	3.3204	10.6870
HMORUN-HLNN	0.9963	2.5663	2.8727	**1.2795**	8.9575
HMORUN-HPLNN	**0.9968**	**2.0579**	**2.6722**	1.7368	**5.9587**

Note: The values in bold indicate the best evaluation metrics values.

the HMORUN-MOSSP stochastic optimization scheduling model proposed in this study can maximize the system's safety and economic efficiency.

3) COMPARISON OF MULTI-OBJECTIVE SCHEDULING MODELS

To verify the performance of the proposed scheduling model, comparative experiments are conducted between the HMORUN-MOSSP, MOALO-MOSSP, MODA-MOSSP, NSGAIII-MOSSP, MOSSA-MOSSP, and MORUN-MOSSP scheduling models, and the experimental results are shown in Fig. 10 and Table 10.

Fig. 10 compares the PF results of various random optimization scheduling models. It can be seen from Fig. 10 that the non-dominated solutions generated by the HMORUN-MOSSP scheduling model are uniformly distributed with high density and a wider solution span, which demonstrates the effectiveness and superiority of

TABLE 7. Statistics on photovoltaic power forecasting results of six neural network forecasting models.

Models	Evaluation metrics				
	IA	MAE	RMSE	SDEX	MdAPE
HMORUN-BPNN	0.9932	2.5564	3.2534	2.0406	**34.5767**
HMORUN-LSTM	0.9932	2.4200	3.0910	1.9636	42.8489
HMORUN-WNN	0.9948	2.2784	2.8125	1.6750	45.3127
HMORUN-RLEM	0.9897	2.8044	3.7694	2.5729	56.2243
HMORUN-HLNN	0.9744	4.1066	6.3381	4.9310	59.8132
HMORUN-HPLNN	**0.9963**	**1.7805**	**2.3713**	**1.5996**	40.0019

Note: The values in bold indicate the best evaluation metrics values.

TABLE 8. Statistical results of SLDI optimization for different combinations of weight ratios for α_1, α_2, and α_3.

α_1	α_2	α_3	Q_P	Q_L	Q_θ	F_{SI}
1	1	1	344.264	5.98E-13	3.35E-05	114.45
2	1	1	345.081	5.50E-13	3.38E-05	152.58
4	1	1	344.052	4.66E-13	3.36E-05	151.24
8	1	1	345.484	4.80E-13	3.39E-05	150.03
1	2	1	345.427	4.39E-13	3.39E-05	85.881
1	4	1	344.480	5.75E-13	3.38E-05	57.374
1	8	1	344.561	5.73E-13	3.38E-05	34.360
1	1	2	345.155	5.40E-13	3.40E-05	85.888
1	1	4	343.695	4.97E-13	3.37E-05	57.373
1	1	8	343.695	4.97E-13	3.37E-05	34.355
1	2	2	345.136	4.02E-13	3.39E-05	68.675
1	4	4	344.547	5.79E-13	3.39E-05	38.144
1	8	8	344.866	5.86E-13	3.38E-05	**20.278**
2	2	1	344.640	6.27E-13	3.38E-05	137.39
4	4	1	344.043	5.21E-13	3.37E-05	152.55
8	8	1	344.739	4.29E-13	3.38E-05	161.84
2	1	2	344.739	5.06E-13	3.38E-05	119.56
4	1	4	344.901	4.05E-13	3.39E-05	98.040
8	1	8	343.827	6.13E-13	3.38E-05	88.495

Note: The values in bold indicate the best values.

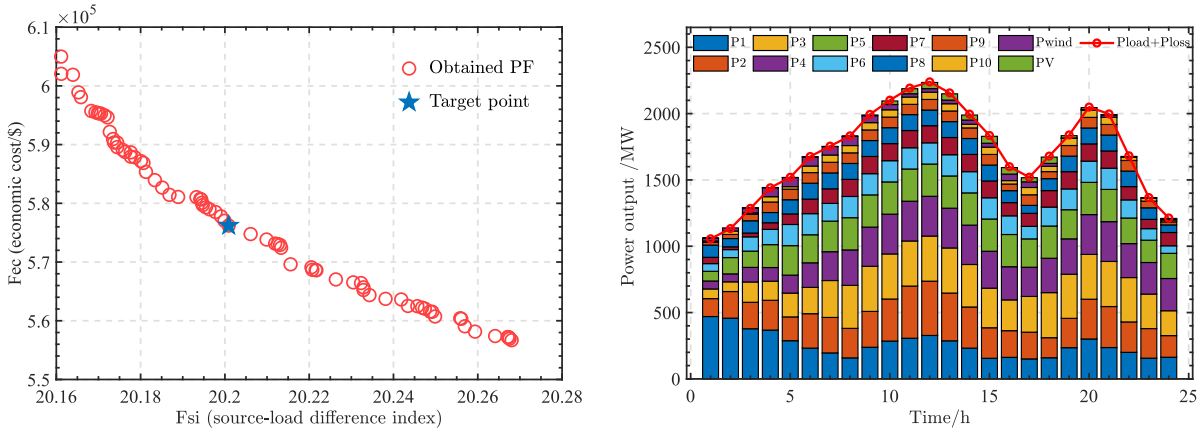

(a) HMORUN Pareto frontier

(b) The optimal compromise output power of the unit

FIGURE 9. The compromise solution selection and optimal output power of units for HMORUN-MOSSP.

using HMORUN to solve the proposed MOSSP problem. Importantly, the solutions generated by the MOALO, MODA, NSGAIII, MOSSA, and MORUN algorithms are dominated by the non-dominated solutions generated by HMORUN,

TABLE 9. The optimal compromise solution for HMORUN.

Hour	P1	P2	P3	P4	P5	P6	P7	P8	P9	P10	Pload	Ploss
1	470.00	135.00	73.01	60.00	73.00	57.89	47.51	92.39	20.00	10.66	1036	19.86
2	457.80	200.77	73.00	60.00	123.00	59.98	21.04	62.39	30.92	19.86	1110	23.08
3	377.80	199.67	153.00	110.00	122.64	107.49	28.91	92.39	49.25	23.08	1258	27.41
4	367.64	224.89	144.02	102.93	172.64	114.93	50.15	77.00	79.25	27.41	1406	34.65
5	287.64	179.53	179.62	135.41	222.23	159.55	79.63	107.00	79.47	34.65	1480	40.07
6	231.82	259.53	198.31	185.41	211.30	159.33	109.63	120.00	80.00	40.07	1628	48.56
7	195.72	267.46	278.31	217.19	230.66	133.41	110.10	120.00	80.00	48.56	1702	52.51
8	158.32	222.36	324.35	267.19	243.00	160.00	128.89	120.00	80.00	52.51	1776	56.09
9	238.32	270.23	340.00	295.55	242.98	160.00	129.81	120.00	80.00	56.09	1924	69.89
10	285.06	316.87	339.96	299.98	243.00	160.00	128.80	120.00	80.00	69.89	2022	79.16
11	306.36	393.28	340.00	299.80	242.98	160.00	129.98	120.00	77.29	79.16	2106	86.17
12	327.29	409.29	340.00	300.00	243.00	160.00	129.21	118.10	79.86	86.17	2150	89.19
13	286.83	360.08	340.00	299.97	243.00	160.00	130.00	119.85	80.00	89.19	2072	83.92
14	231.77	310.14	320.52	296.77	243.00	160.00	130.00	120.00	79.98	83.92	1924	71.86
15	155.09	230.14	298.60	278.47	243.00	160.00	126.81	120.00	80.00	71.86	1776	59.05
16	162.13	201.20	232.10	250.00	243.00	140.84	99.68	90.00	50.00	59.05	1554	45.79
17	150.57	201.45	269.47	220.14	213.81	94.16	98.39	60.00	80.00	45.79	1480	40.76
18	159.21	151.10	340.00	259.08	243.00	142.76	124.33	90.00	53.26	40.76	1628	51.52
19	235.09	221.22	332.60	266.69	219.69	156.88	130.00	117.29	80.00	51.52	1776	62.85
20	300.66	299.95	337.89	299.99	243.00	160.00	130.00	120.00	80.00	62.85	1972	77.10
21	236.19	309.12	340.00	300.00	243.00	160.00	130.00	120.00	79.97	77.10	1924	73.35
22	200.12	229.12	334.54	255.90	193.03	136.77	100.00	117.16	80.00	73.35	1628	53.85
23	156.02	223.15	260.02	238.18	168.29	86.77	70.00	87.16	50.61	53.85	1332	35.08
24	163.18	162.99	187.48	242.99	189.89	57.00	100.00	57.16	23.23	35.08	1184	28.95

TABLE 10. Statistics of experimental results for six models of SLDI and economic costs.

	MOALO-MOSSP	MODA-MOSSP	NSGAIII-MOSSP	MOSSA-MOSSP	MORUN-MOSSP	HMORUN-MOSSP
SLDI	20.2544	20.2637	20.2911	20.2356	20.2221	**20.2009**
Cost ($)	613096.76	623262.31	618789.15	604965.89	591294.18	**576205.58**

Note: The values in bold indicate the best values.

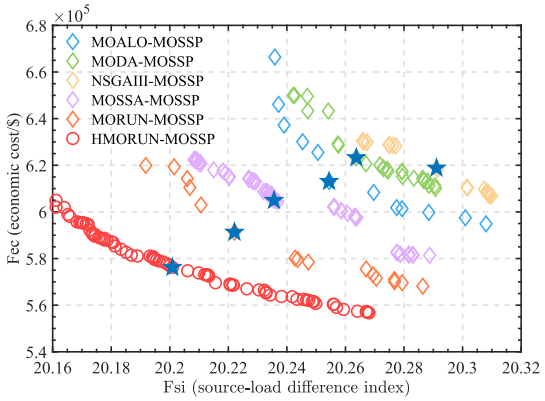

FIGURE 10. Comparison of the Pareto frontier of six stochastic optimal scheduling models.

which indicates that the non-dominated solutions obtained by HMORUN in solving MOSSP possess higher safety and better economy.

Table 10 presents the statistical results of the multi-objective scheduling model SLDI and the economic costs experiment. The results indicate that the SLDI and economic cost values obtained by the HMORUN-MOSSP scheduling model (20.2009 and 576205.58, respectively) are better than those obtained by the comparison models.

The comprehensive experimental results demonstrate that the performance of the proposed HMORUN-MOSSP scheduling model is significantly better than that of the MOALO-MOSSP, MODA-MOSSP, NSGAIII-MOSSP, MOSSA-MOSSP, and MORUN-MOSSP scheduling models.

VI. CONCLUSION

In this study, a stochastic optimization scheduling model for integrated multi-objective forecasting, scenario generation, and decision scheduling based on HPLNN, HMORUN, LHS, SBR, and MOSSP is proposed. Through extensive and comprehensive experiments, the following conclusions can be drawn:

Under the same experimental conditions, the proposed HMORUN-HPLNN forecasting model has significant advantages over the HMORUN-HLNN forecasting model for wind power and photovoltaic generation forecasting. HPLNN can overcome the limitations of traditional feedforward neural networks and thus improve the forecasting performance of the model.

The proposed HMORUN algorithm shows significant advantages over other advanced algorithms in solving multi-objective forecasting problems. In multi-objective wind and photovoltaic power forecasting problems, the

HMORUN-HPLNN prediction model outperforms the MOALO-HPLNN, MODA-HPLNN, NSGAIII-HPLNN, MOSSA-HPLNN, and MORUN-HPLNN forecasting models in terms of forecasting accuracy and stability. Overall, HMORUN demonstrates promising applications in multi-objective wind and photovoltaic power forecasting.

The proposed HMORUN-MOSSP stochastic optimization scheduling model ensures both safety and economy of scheduling results while also minimizing the amount of wind and photovoltaic power curtailment and load shedding. Compared with other multi-objective scheduling models, the non-dominated solution distribution of the HMORUN-MOSSP scheduling model is more uniform and has a higher distribution density, and the solutions generated by MOALO, MODA, NSGAIII, MOSSA, and MORUN algorithms are dominated by the non-dominated solutions generated by HMORUN. The non-dominated solutions obtained by the HMORUN-MOSSP algorithm have higher safety and better economy. In the future, a more comprehensive consideration of the uncertainty of renewable energy and load can be made to make the scheduling results safer and more economical.

COMPLIANCE WITH ETHICAL STANDARDS

Conflict of interest: The authors declare that they have no conflict of interest.

Ethical approval: This article does not contain any studies with human participants or animals performed by any of the authors.

Informed consent: Informed consent was obtained from all individual participants included in the study.

REFERENCES

[1] Y. Dong, H. Zhang, P. Ma, C. Wang, and X. Zhou, "A hybrid robust-interval optimization approach for integrated energy systems planning under uncertainties," *Energy*, vol. 274, Jul. 2023, Art. no. 127267.

[2] X. Zhang, W. Huang, S. Chen, D. Xie, D. Liu, and G. Ma, "Grid–source coordinated dispatching based on heterogeneous energy hybrid power generation," *Energy*, vol. 205, Aug. 2020, Art. no. 117908.

[3] H. Wu, X. Liu, and M. Ding, "Dynamic economic dispatch of a microgrid: Mathematical models and solution algorithm," *Int. J. Electr. Power Energy Syst.*, vol. 63, pp. 336–346, Dec. 2014.

[4] M. H. Hassan, S. Kamel, A. Eid, L. Nasrat, F. Jurado, and M. F. Elnaggar, "A developed eagle-strategy supply-demand optimizer for solving economic load dispatch problems," *Ain Shams Eng. J.*, vol. 14, no. 5, May 2023, Art. no. 102083.

[5] Y. Wang, J. Wang, M. Cao, X. Kong, B. Abderrahim, L. Yuan, and A. Vartosh, "Dynamic emission dispatch considering the probabilistic model with multiple smart energy system players based on a developed fuzzy theory-based harmony search algorithm," *Energy*, vol. 269, Apr. 2023, Art. no. 126417.

[6] H. Qiu, W. Gu, P. Liu, Q. Sun, Z. Wu, and X. Lu, "Application of two-stage robust optimization theory in power system scheduling under uncertainties: A review and perspective," *Energy*, vol. 251, Jul. 2022, Art. no. 123942.

[7] X. Chen and X. Wu, "The roles of carbon capture, utilization and storage in the transition to a low-carbon energy system using a stochastic optimal scheduling approach," *J. Cleaner Prod.*, vol. 366, Sep. 2022, Art. no. 132860.

[8] M. S. Li, Z. J. Lin, T. Y. Ji, and Q. H. Wu, "Risk constrained stochastic economic dispatch considering dependence of multiple wind farms using pair-copula," *Appl. Energy*, vol. 226, pp. 967–978, Sep. 2018.

[9] W. Liu, F. Zhu, T. Zhao, H. Wang, X. Lei, P.-A. Zhong, and V. Fthenakis, "Optimal stochastic scheduling of hydropower-based compensation for combined wind and photovoltaic power outputs," *Appl. Energy*, vol. 276, Oct. 2020, Art. no. 115501.

[10] M. Rahimi, F. J. Ardakani, and A. J. Ardakani, "Optimal stochastic scheduling of electrical and thermal renewable and non-renewable resources in virtual power plant," *Int. J. Electr. Power Energy Syst.*, vol. 127, May 2021, Art. no. 106658.

[11] K. Li, F. Yang, L. Wang, Y. Yan, H. Wang, and C. Zhang, "A scenario-based two-stage stochastic optimization approach for multi-energy microgrids," *Appl. Energy*, vol. 322, Sep. 2022, Art. no. 119388.

[12] F. Mei, J. Zhang, J. Lu, J. Lu, Y. Jiang, J. Gu, K. Yu, and L. Gan, "Stochastic optimal operation model for a distributed integrated energy system based on multiple-scenario simulations," *Energy*, vol. 219, Mar. 2021, Art. no. 119629.

[13] A. Staid, J. Watson, R. J. Wets, and D. L. Woodruff, "Generating short-term probabilistic wind power scenarios via nonparametric forecast error density estimators," *Wind Energy*, vol. 20, no. 12, pp. 1911–1925, Dec. 2017.

[14] Z. Lin, H. Chen, Q. Wu, W. Li, M. Li, and T. Ji, "Mean-tracking model based stochastic economic dispatch for power systems with high penetration of wind power," *Energy*, vol. 193, Feb. 2020, Art. no. 116826.

[15] S. Delikaraoglou and P. Pinson, "High-quality wind power scenario forecasts for decision-making under uncertainty in power systems," in *Proc. 13th Int. Workshop Large-Scale Integr. Wind Power Power Syst. Transmiss. Netw. Offshore Wind Power*, 2014, pp. 8885–8950.

[16] M. Cui, D. Ke, Y. Sun, D. Gan, J. Zhang, and B.-M. Hodge, "Wind power ramp event forecasting using a stochastic scenario generation method," *IEEE Trans. Sustain. Energy*, vol. 6, no. 2, pp. 422–433, Apr. 2015.

[17] Y. Chen, Y. Wang, D. Kirschen, and B. Zhang, "Model-free renewable scenario generation using generative adversarial networks," *IEEE Trans. Power Syst.*, vol. 33, no. 3, pp. 3265–3275, May 2018.

[18] M. Rayati, M. Bozorg, M. Carpita, and R. Cherkaoui, "Stochastic optimization and Markov chain-based scenario generation for exploiting the underlying flexibilities of an active distribution network," *Sustain. Energy, Grids Netw.*, vol. 34, Jun. 2023, Art. no. 100999.

[19] S. I. Vagropoulos, E. G. Kardakos, C. K. Simoglou, A. G. Bakirtzis, and J. P. S. Catalão, "ANN-based scenario generation methodology for stochastic variables of electric power systems," *Electr. Power Syst. Res.*, vol. 134, pp. 9–18, May 2016.

[20] N. M. Moraes, U. H. Bezerra, J. L. M. Rodríguez, M. H. R. Nascimento, and J. C. Leite, "A new approach to economic-emission load dispatch using NSGA II. Case study," *Int. Trans. Electr. Energy Syst.*, vol. 28, no. 11, p. e2626, Nov. 2018.

[21] M. H. R. Nascimento, M. V. A. Nunes, J. L. M. Rodríguez, and J. C. Leite, "A new solution to the economical load dispatch of power plants and optimization using differential evolution," *Electr. Eng.*, vol. 99, no. 2, pp. 561–571, Jun. 2017.

[22] X. Li, W. Wang, H. Wang, J. Wu, X. Fan, and Q. Xu, "Dynamic environmental economic dispatch of hybrid renewable energy systems based on tradable green certificates," *Energy*, vol. 193, Feb. 2020, Art. no. 116699.

[23] C. G. Marcelino, G. M. C. Leite, C. A. D. M. Delgado, L. B. de Oliveira, E. F. Wanner, S. Jiménez-Fernández, and S. Salcedo-Sanz, "An efficient multi-objective evolutionary approach for solving the operation of multi-reservoir system scheduling in hydro-power plants," *Expert Syst. Appl.*, vol. 185, Dec. 2021, Art. no. 115638.

[24] J. Ye, L. Xie, L. Ma, Y. Bian, and X. Xu, "A novel hybrid model based on Laguerre polynomial and multi-objective Runge–Kutta algorithm for wind power forecasting," *Int. J. Electr. Power Energy Syst.*, vol. 146, Mar. 2023, Art. no. 108726.

[25] Q. Zhang, X. Wang, T. Yang, and J. Liang, "Research on scheduling optimisation for an integrated system of wind-photovoltaic-hydro-pumped storage," *J. Eng.*, vol. 2017, no. 13, pp. 1210–1214, Jan. 2017.

[26] C. Peng, P. Xie, L. Pan, and R. Yu, "Flexible robust optimization dispatch for hybrid wind/photovoltaic/hydro/thermal power system," *IEEE Trans. Smart Grid*, vol. 7, no. 2, pp. 751–762, Mar. 2016.

[27] L. Ye, H. B. Sun, X. R. Song, and L. C. Li, "Dynamic modeling of a hybrid wind/solar/hydro microgrid in EMTP/ATP," *Renew. Energy*, vol. 39, no. 1, pp. 96–106, Mar. 2012.

[28] Y. Zhu, S. Chen, W. Huang, L. Wang, and G. Ma, "Complementary operational research for a hydro-wind-solar hybrid power system on the upper Jinsha River," *J. Renew. Sustain. Energy*, vol. 10, no. 4, Jul. 2018, Art. no. 043309.
[29] X. Wang, Y. Mei, Y. Kong, Y. Lin, and H. Wang, "Improved multi-objective model and analysis of the coordinated operation of a hydro-wind-photovoltaic system," *Energy*, vol. 134, pp. 813–839, Sep. 2017.
[30] B. Ming, P. Liu, S. Guo, X. Zhang, M. Feng, and X. Wang, "Optimizing utility-scale photovoltaic power generation for integration into a hydropower reservoir by incorporating long- and short-term operational decisions," *Appl. Energy*, vol. 204, pp. 432–445, Oct. 2017.
[31] J. Xu, F. Wang, C. Lv, and H. Xie, "Carbon emission reduction and reliable power supply equilibrium based daily scheduling towards hydro-thermal-wind generation system: A perspective from China," *Energy Convers. Manage.*, vol. 164, pp. 1–14, May 2018.
[32] Z. Yang, P. Liu, L. Cheng, H. Wang, B. Ming, and W. Gong, "Deriving operating rules for a large-scale hydro-photovoltaic power system using implicit stochastic optimization," *J. Cleaner Prod.*, vol. 195, pp. 562–572, Sep. 2018.
[33] Y. Dong, H. Zhang, C. Wang, and X. Zhou, "Wind power forecasting based on stacking ensemble model, decomposition and intelligent optimization algorithm," *Neurocomputing*, vol. 462, pp. 169–184, Oct. 2021.
[34] C. Wang, H. Zhang, and P. Ma, "Wind power forecasting based on singular spectrum analysis and a new hybrid Laguerre neural network," *Appl. Energy*, vol. 259, Feb. 2020, Art. no. 114139.
[35] G. E. Hinton, S. Osindero, and Y.-W. Teh, "A fast learning algorithm for deep belief nets," *Neural Comput.*, vol. 18, no. 7, pp. 1527–1554, Jul. 2006.
[36] P. Guo and M. R. Lyu, "A pseudoinverse learning algorithm for feedforward neural networks with stacked generalization applications to software reliability growth data," *Neurocomputing*, vol. 56, pp. 101–121, Jan. 2004.
[37] I. Ahmadianfar, A. A. Heidari, A. H. Gandomi, X. Chu, and H. Chen, "RUN beyond the metaphor: An efficient optimization algorithm based on Runge Kutta method," *Expert Syst. Appl.*, vol. 181, Nov. 2021, Art. no. 115079.
[38] K. Deb, A. Pratap, S. Agarwal, and T. Meyarivan, "A fast and elitist multiobjective genetic algorithm: NSGA-II," *IEEE Trans. Evol. Comput.*, vol. 6, no. 2, pp. 182–197, Apr. 2002.
[39] J. Bourcet, A. Kubilay, D. Derome, and J. Carmeliet, "Representative meteorological data for long-term wind-driven rain obtained from Latin hypercube sampling—Application to impact analysis of climate change," *Building Environ.*, vol. 228, Jan. 2023, Art. no. 109875.
[40] H. Heitsch and W. Römisch, "Scenario reduction algorithms in stochastic programming," *Comput. Optim. Appl.*, vol. 24, nos. 2–3, pp. 187–206, Feb. 2003.
[41] Y. Zhu, B. Qiao, Y. Dong, B. Qu, and D. Wu, "Multiobjective dynamic economic emission dispatch using evolutionary algorithm based on decomposition," *IEEJ Trans. Electr. Electron. Eng.*, vol. 14, no. 9, pp. 1323–1333, Sep. 2019.
[42] S. Mouassa and T. Bouktir, "Multi-objective ant lion optimization algorithm to solve large-scale multi-objective optimal reactive power dispatch problem," *COMPEL-Int. J. Comput. Math. Electr. Electron. Eng.*, vol. 38, no. 1, pp. 304–324, Jan. 2019.
[43] S. Mirjalili, "Dragonfly algorithm: A new meta-heuristic optimization technique for solving single-objective, discrete, and multi-objective problems," *Neural Comput. Appl.*, vol. 27, no. 4, pp. 1053–1073, May 2016.
[44] K. Deb and H. Jain, "An evolutionary many-objective optimization algorithm using reference-point-based nondominated sorting approach, Part I: Solving problems with box constraints," *IEEE Trans. Evol. Comput.*, vol. 18, no. 4, pp. 577–601, Aug. 2014.
[45] S. Mirjalili, A. H. Gandomi, S. Z. Mirjalili, S. Saremi, H. Faris, and S. M. Mirjalili, "Salp swarm algorithm: A bio-inspired optimizer for engineering design problems," *Adv. Eng. Softw.*, vol. 114, pp. 163–191, Dec. 2017.
[46] S. Wang, N. Zhang, L. Wu, and Y. Wang, "Wind speed forecasting based on the hybrid ensemble empirical mode decomposition and GA-BP neural network method," *Renew. Energy*, vol. 94, pp. 629–636, Aug. 2016.
[47] Y. Yu, X. Si, C. Hu, and J. Zhang, "A review of recurrent neural networks: LSTM cells and network architectures," *Neural Comput.*, vol. 31, no. 7, pp. 1235–1270, Jul. 2019.
[48] S. Jafarzadeh Ghoushchi, S. Manjili, A. Mardani, and M. K. Saraji, "An extended new approach for forecasting short-term wind power using modified fuzzy wavelet neural network: A case study in wind power plant," *Energy*, vol. 223, May 2021, Art. no. 120052.
[49] E. H. Field, "Overview of the working group for the development of regional earthquake likelihood models (RELM)," *Seismolog. Res. Lett.*, vol. 78, no. 1, pp. 7–16, Jan. 2007.